CHEMISTRY OF MATERIALS
Article
pubs.acs.org/cm

Structural, Optical, and Transport Properties of α- and β-Ag_3VO_4

V. Cloet,[†] A. Raw,[†] K. R. Poeppelmeier,[*,†] G. Trimarchi,[‡] H. Peng,[‡] J. Im,[‡] A.J. Freeman,[‡] N. H. Perry,[§] T. O. Mason,[§] A. Zakutayev,[¶] P. F. Ndione,[¶] D. S. Ginley,[¶] and J. D. Perkins[¶]

[†]Department of Chemistry, [‡]Department of Physics and Astronomy, and [§]Department of Materials Science and Engineering, Northwestern University, Evanston, Illinois 60208, United States

[¶]National Renewable Energy Laboratory, Golden, Colorado 80401, United States

S Supporting Information

ABSTRACT: The structures of α- and β-Ag_3VO_4 were studied via single-crystal X-ray diffraction (XRD). The transition from α-phase to β-phase was found to occur at 110 °C. Single-crystal XRD revealed that the integrity of the single crystals was maintained as Ag_3VO_4 reversibly transitioned between α-Ag_3VO_4 and β-Ag_3VO_4. The optical and electrical properties of polycrystalline α-Ag_3VO_4 were studied by diffuse reflectance spectroscopy and impedance spectroscopy. In order to assess the optical and electrical properties of β-Ag_3VO_4, *in situ* measurements were performed above the phase-transition temperature. Thin films of α-Ag_3VO_4 were prepared by combinatorial sputtering and pulsed laser deposition (PLD). The crystallographic, optical, and electrical conductivity properties of the α-Ag_3VO_4 thin films were compared with the bulk properties.

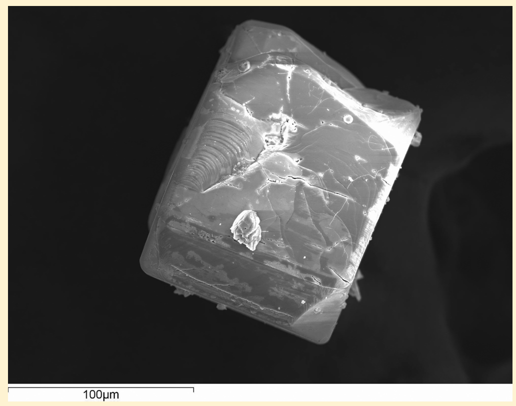

KEYWORDS: *α-Ag_3VO_4, β-Ag_3VO_4, single crystal, thin film, electrical conductivity*

INTRODUCTION

Ternary silver oxides with Ag^+ ions have been studied for their unique crystal structures.[1−4] Dictated by the nature of their chemical bonding, compounds with d^{10} Ag^+ ions have been observed to exhibit several interesting properties. Photocatalytic and photochromic properties have been reported previously by Hirono et al.[1] and were found in a broad range of ternary Ag compounds such as $AgGaO_2$,[5−7] Ag_4SiO_4,[8,9] and Ag_3PO_4.[10−12] In addition, Ag_3VO_4 has been studied by several groups as potential photocatalysts.[13−16]

Ag_3VO_4 has been observed in three polymorphs: α-, β- (famatinite structure), and γ-Ag_3VO_4.[13] Previously, the β- and γ-phases have only been characterized by powder X-ray diffraction (XRD). The low-temperature α-phase of Ag_3VO_4 forms a structure type that has not been observed previously in other AB_3X_4 systems. In all three polymorphs of this noble-metal oxovanadate, both the noble metal and the vanadium cations are 4-fold coordinated by oxygen.

Apart from exhibiting photocatalytic properties, α-Ag_3VO_4 was considered previously as a potential *p*-type transparent conductor.[17] This earlier research focused on the theoretical predictions of the optical and electrical properties of α-Ag_3VO_4. Calculations illustrate that the formation energy of oxygen vacancies in Ag_3VO_4 is high and that oxygen vacancies do not compensate for the Ag cation vacancies. As a result, holes are formed, a required target property for a *p*-type conductor. Because theoretical calculations predicted a higher optical (indirect) band gap for β-Ag_3VO_4 (2.67 eV) than for α-Ag_3VO_4 (2.4 eV), stabilizing the β-phase could be an interesting route to obtain a transparent *p*-type conducting oxide. However, the stabilization of β-Ag_3VO_4 remains challenging. The low phase-transition temperature from α-Ag_3VO_4 to β-Ag_3VO_4 (at 110 °C) and the photoinduced reverse phase transition prevent the stabilization of β-Ag_3VO_4 at room temperature. Therefore, the assessment of the optical and electrical properties of β-Ag_3VO_4 was not possible at room temperature. Instead, we measured these properties *in situ* on sintered polycrystalline samples above the phase-transition temperature.

Another possibility to stabilize β-Ag_3VO_4 is to strain it by depositing thin films on textured substrates. One earlier publication was successful in stabilizing β-Ag_3VO_4 at room temperature by depositing thin films through anodic oxidation on quartz glass substrates.[18] In this publication, thin films of α-Ag_3VO_4 were grown by pulsed laser deposition (PLD) and combinatorial sputtering on sapphire, amorphous silica, and YSZ substrates. However, β-Ag_3VO_4 could not be stabilized in thin films.

The *in situ* analysis of polycrystalline pellets of Ag_3VO_4 revealed that, in accordance to the theoretical predictions, the absorption onset of β-Ag_3VO_4 is slightly higher than that of α-Ag_3VO_4. The electrical conductivity of β-Ag_3VO_4 was also higher than the conductivity in α-Ag_3VO_4. However, because of

Received: April 10, 2012
Revised: August 1, 2012
Published: August 1, 2012

the near-perfect stoichiometry of Ag_3VO_4, the concentration of cation vacancies is too low to make it a sizable *p*-type conductor. Extrinsic hole doping could provide a solution to this problem, but the presence of polarons do not favor such doping. In addition to the analyses on polycrystalline samples, the reversible α-phase to β-phase transition was observed in a single crystal of Ag_3VO_4. This provides more-detailed structural information of the β-phase, which is of paramount importance to understand the impact of structural features on properties of materials. Both PLD and combinatorial sputtering were successful in synthesizing thin films of α-Ag_3VO_4, but β-Ag_3VO_4 films were not stabilized at room temperature. The range of growth conditions such as temperature, pressure, and cation stoichiometry needed to obtain thin films of α-Ag_3VO_4 was very narrow. Large variations in phase purity was observed in the thin films as growth conditions changed only slightly. This suggests that α-Ag_3VO_4 films grown by physical vapor deposition techniques disproportionate easily. This, together with the study of the stability diagram of Ag_3VO_4, illustrates that freezing the β-phase is very challenging and should be approached via a different route.

■ EXPERIMENTAL SECTION

Synthesis. *Caution! Hydrofluoric acid (HF) is toxic and corrosive and must be handled with extreme caution and the appropriate protective equipment. If contact with the liquid or vapor occurs, proper treatment procedures should be followed immediately.*[19−21]

Single crystals of α-Ag_3VO_4 were formed by hydrothermal reaction through the use of hydrofluoric acid as a mineralizer. Ag_2O (Fisher Chemical, laboratory grade), V_2O_5 (Alfa Aesar, 99.6% minimum) and hydrofluoric acid (Fisher, 48%−50% HF by weight) were combined in a 1:8:20 molar ratio in a fluoro(ethylene-propylene) (FEP) Teflon pouch.[22] The pouches were heat-sealed and up to five were loaded in a 125-mL autoclave with a Teflon liner. The sealed autoclave was heated to 150 °C for 24 h and cooled at a rate of 0.1 °C/min to facilitate crystal growth. After synthesis, products were vacuum filtered to remove the remaining HF. The single crystals were large (0.1 mm^3) and had a red color. The small crystal size did not allow for the direct measurement of optical and electrical properties. The synthesis of polycrystalline Ag_3VO_4 was described in detail in our previous publication.[17]

Films 200−300 nm thick, with a composition gradient in the Ag/V ratio, were grown using reactive magnetron cosputtering from Ag and V metallic targets in the presence of a mixture of argon and oxygen gases. The ratio of Ar/O_2 flow was fixed to 10/10 sccm during growth. Sputter guns were pointed at 45° with respect to the 50 mm × 50 mm glass substrates in order to achieve a well-controlled, intentional gradient of cation chemical composition. The substrate temperature during the growth was varied over the temperature range of 50−500 °C, with the goal being to identify the optimal growth conditions for the α-Ag_3VO_4 phase. The growth at the optimal temperature range (350−450 °C) was repeated 2−3 times to check the reproducibility of the results. More details on the combinatorial approach to the thin film growth can be found elsewhere.[23]

Thin films were also grown on amorphous fused silica, (0001) Al_2O_3, and (100) YSZ substrates via pulsed laser deposition (PLD), using a high-vacuum deposition chamber and a KrF excimer laser (Spectra-Physics operating at 248 nm with a pulse duration of 25 ns).[24] The laser was operated at 10 Hz and the beam was focused through a 40 cm lens onto a 1 in. pressed pellet of α-Ag_3VO_4 rotating target (the polycrystalline α-Ag_3VO_4 target was prepared using the method described earlier[17]) at a 45° angle, thus obtaining a laser fluence of 3 J cm^{-2} on the target surface. The target−substrate distance was fixed at 4 cm. Prior to the deposition, the growth chamber was evacuated to a base pressure of 10^{-6} Torr, using a turbomolecular pump. Depositions were performed at a substrate temperature varying from 32 °C to 450 °C under an oxygen reactive pressure in the range of 2−200 mTorr. The number of laser pulses between depositions was varied in such a way that a similar thickness of 150 nm could be obtained for all films.

Crystallographic Studies. Powder XRD patterns of the polycrystalline samples were obtained from a Rigaku Model XDS 2000 diffractometer with Ni-filtered Cu Kα radiation (λ = 1.5418 Å) at 40 kV and 20 mA. Data were collected between 15° and 65° at a step size of 0.05° and a dwell time of 0.8 s. The XRD patterns were compared with the JCPDS files (α-Ag_3VO_4, File Card No. 43-0542; β-Ag_3VO_4, File Card No. 43-0543), using the Jade9 software suite.[25]

Low-temperature single-crystal XRD data for Ag_3VO_4 were collected with the use of graphite-monochromatized Mo Kα radiation (λ = 0.71073 Å) at −173 °C (100 K) on a Bruker APEX2 diffractometer with a SMART CCD area detector.[26,27] The 0.1 mm^3 single crystals were grown by the hydrofluoric acid method as described above. The crystal-to-detector distance was 50 mm. The data collection strategy and the collection of intensity data, as well as cell refinement and data reduction, were carried out with the use of the program APEX2.[26,27] Face-indexed absorption, incident beam, and decay corrections were performed with the use of the program SADABS.[28,29] For the elevated temperature experiment, single-crystal XRD data were collected on the same single crystals at 127 °C (400 K) by performing ω scans on a STOE IPDS II diffractometer using Mo Kα radiation (λ = 0.71073 Å) operating at 50 kV and 40 mA. Collection, integration, and numerical absorption corrections were performed using the X-AREA, X-RED and X-SHAPE programs.[30] The structure was solved with the direct-methods program SHELXS and refined with the full-matrix least-squares program SHELXL.[31] Each final refinement included anisotropic displacement parameters. The program STRUCTURE TIDY was used to standardize the positional parameters.[32]

Each thin film grown by combinatorial sputtering was characterized at 44 spatial locations arranged on the 4 × 11 rectangular grid. All thin films were measured for chemical composition and thickness using X-ray fluorescence (XRF) and for crystalline phase composition using X-ray diffraction (XRD) (Bruker Discovery 08) using a HI-STAR area detector. The thickness of the PLD films was determined by spectroscopic ellipsometry (J. A. Woollam, No. M-2000S).

Optical Studies. A Perkin−Elmer Model Lambda1050 instrument with an integrating sphere was used to collect diffuse reflectance data of the polycrystalline sample over the spectral range of 250−800 nm with a data interval of 1 nm. A baseline was collected using a slit width of 2 mm at 650 nm. The value of the band gap is obtained by fitting a line to the high-energy edge of the top of the diffuse reflectance and taking the intersection of this line with the fitted curve to the low-energy end of the spectrum. This method of band-gap estimation is valid for powders and thick coatings and is based on the Kubelka−Munk model.[33] The *in situ* diffuse reflectance spectroscopy was performed on a Harrick Praying Mantis mounted with a reaction cell in a range from 25 and 200 °C. The optical properties of the films were determined using two coupled Ocean Optics spectrometers that measure transmittance and reflectance over the range of 330−1000 nm.

Electrical Studies. AC impedance spectroscopy, using an HP 4192A impedance analyzer (Agilent Technologies, Santa Clara, CA), was used to measure the temperature-dependent electrical conductivity and dielectric constant of the pressed and sintered polycrystalline Ag_3VO_4 pellet synthesized under basic conditions. Silver electrodes were attached on both faces of the pellet, which was held in a tube furnace in ambient air. Inductive contributions from the setup were minimized by using separate current and voltage leads, which were also individually shielded and grounded to avoid capacitive contributions. In addition, the electrodes were either sputtered or painted (rather than just mechanically attached to the sample) to avoid spreading resistance contributions.[34] The temperature was increased from 25 °C to 400 °C in steps of 25 °C. The measurements were made after equilibrating at each temperature for 30 min, and temperatures were monitored with an S-type thermocouple. Impedance spectra were fit using the nonlinear least-squares algorithm in Boukamp's Equivalent Circuit program[35] using the appropriate circuit, i.e., $LR_1(R_2Q)$ for the single arc behavior observed at all temperatures. L and R_1 respectively represent inductance and resistance from the setup (leads); R_2 represents the total resistance of the sample, and the constant phase element Q is related to the capacitance of the sample as

$$C = (R^{1-n}Q)^{1/n}$$

Arc depression was minimal; values for the constant phase element parameter n ranged from 0.89 to 1, with the lower values occurring only at and just above the phase-transition temperature, possibly indicating the temporary presence of both phases. The fitted resistances and capacitances were corrected for sample geometry and porosity to obtain values for the conductivity and dielectric constant. (For highly dense samples, the resistance R_2 can be corrected for porosity (f = fraction porosity) using Maxwell's dilute limit equation,[36]

$$R_{\text{dense}} = R_{\text{porous}}\left(1 - \frac{3}{2}f\right)$$

The capacitance C can then be corrected by assuming that the time constant, $\tau = RC$, remains unaffected by the correction. In this case, such corrections were negligible, because of the high density of the sample, measured as 5.73 g/cm^3). From the porosity-corrected capacitance (C^{pc}) and the permittivity of free space (ε_0), the effective dielectric constant was determined as $\varepsilon = (C^{\text{pc}}/\varepsilon_0)(L/A)$, where L is the sample length or thickness and A is its cross-sectional area. The electrical conductivity of the thin films of α-Ag_3VO_4 was analyzed using collinear 4-point probe sheet resistance measurements.[37] Sheet resistance was determined using the equation

$$R_s = 2\pi sFR$$

where s is the spacing between the voltage measurement tips, F the correction factor that takes into account that the thickness of the samples is much smaller than the distance between the tips ($F = 1/(2\ln(2))$, and R the measured resistance. The head was connected to a Keithley 2000 multimeter set in the 4-wire measurement mode. Current was passed through the two outer tips and voltage was measured across two inner tips. A Signatone SP4 spring-loaded linear four-point-probe head was used for these measurements. The spacing between the cylindrical tungsten carbide tips was 1 mm and their diameter was 0.08 mm.

Crystallographic Structure of β-Ag_3VO_4. To date, three polymorphs of Ag_3VO_4 have been reported.[13,16] At room temperature, α-Ag_3VO_4 is the stable polymorph, β-Ag_3VO_4 is stable between 110 °C and 414 °C, and γ-Ag_3VO_4 is stable from 414 °C to 530 °C. α-Ag_3VO_4 crystallizes in a monoclinic structure (space group $C2/c$), whereas the β-phase adopts the tetragonal famatinite structure (Cu_3SbS_4, space group $I\bar{4}2m$). The γ-phase belongs to the cubic crystal structure (space group $F\bar{4}3m$), but was not further investigated.

The α-phase is a unique structure and has not been observed in other A_3XB_4 compounds.[13,16] The α-phase and β-phase (famatinite structure), however, can be derived from the fcc lattice. In both structures, the A and B cations order along the (201) direction of the fcc lattice with the A_3B_1 stacking sequence, while the O-atoms occupy tetrahedral interstitial sites of the fcc lattice. In the fcc lattice, there are two symmetrically distinct sets of tetrahedral interstitial sites, obtained starting from the fcc lattice and applying $(^1/_4, ^1/_4, ^1/_4)a_{\text{tot}}$ and $(-^1/_4, ^1/_4, ^1/_4)a_{\text{tot}}$ translations; these are referenced here as, respectively, $T^{(+)}$ and $T^{(-)}$. In α-Ag_3VO_4, the oxide anions within an fcc conventional cell occupy only tetrahedral interstitials of a given type, e.g., $T^{(+)}$. Moving to the next adjacent cell, the anions occupy the other interstitials, e.g., $T^{(-)}$.[16] This arrangement leads to the presence of three symmetry unique cation sites with different coordination geometries: first, the V sites, which are tetrahedrally coordinated; second, the seesaw Ag-sites, in which two of the four nearest-neighbor oxygen form a linear O-M-O unit, while the other two ligands form roughly perpendicular bonds to the O−M−O unit and last, the distorted square planar Ag sites. The average silver oxygen bond distance is 2.367 Å for the square planar silver (Wyckoff position 8f) with O−Ag−O bond angles ranging from 81° to 98° but maintaining the 180° angle between trans oxygen expected in the square planar configuration. This bond distance is long in comparison to the silver oxygen bond distance (1.935 Å) measured in AgO^- by negative-ion photoelectron spectroscopy.[38] This difference can be attributed to the different environments of both Ag−O bonds. In the case of Ag_3VO_4, the bond distance is measured in a three-dimensional (3D) crystal surrounded by other atoms, whereas Lineberger et al. measured the Ag−O bond distance in a single AgO^- molecule. For the silver ions in a seesaw configuration (Wyckoff position 4a) the average Ag−O bond distance is 2.330 Å with a 177° angle for the linear O−Ag−O bond and an angle of 93° between the other two oxygen ions.

α-Ag_3VO_4, upon heating to 110 °C, transitions to β-Ag_3VO_4, where both cations are tetrahedrally coordinated. Upon cooling, the β-form returns to the α-structure with a slight degradation in crystal quality. We report, for the first time, the refined atomic positions of β-Ag_3VO_4 with corresponding anisotropic displacement parameters. This was achieved by performing *in situ* single-crystal XRD (see Table 1 for details). Single-crystal XRD was performed at 127 °C. At this temperature, a complete phase transition to β-Ag_3VO_4 is ensured. The results of the crystallographic refinements of α and β-Ag_3VO_4 and their comparison to the values for α-Ag_3VO_4 reported from previous powder studies can be seen in Table 2. In the famatinite structure, there are two tetrahedral Ag sites with Ag−O bond lengths of 2.3082 Å (Wyckoff position 4d), and 2.335 Å (Wyckoff position 2b). These lengths are comparable with the bond distances of 2.325 Å and 2.377

Table 1. Comparison of Atomic Positions from Powder Diffraction[13] and from Single-Crystal Diffraction[a]

	x	y	z	U
		Powder Diffraction		
Ag(1)	0	0	0.5	0.1927(20)
Ag(2)	0	0.5	0.75	0.1925(16)
V	0	0	0	0.0316(20)
O	0.1927(5)	0.1927(5)	0.0997(5)	0.0057(16)
		Single-Crystal Diffraction		
Ag(1)	0	0	0.5	0.0845(9)
Ag(2)	0	0.5	0.75	0.0725(6)
V	0	0	0	0.0280(6)
O	0.1992(10)	0.1992(10)	0.1010(7)	0.0404(17)

[a]Note: the literature values have been standardized by the program STRUCTURE TIDY for better comparison.[39]

Table 2. Comparison between Single-Crystal Refinement and the Reported Values for Polycrystalline Ag_3VO_4[13]

	α-Ag_3VO_4	β-Ag_3VO_4	literature β-Ag_3VO_4
crystal system	monoclinic	tetragonal	tetragonal
space group	$C2/c$	$I\bar{4}2m$	$I\bar{4}2m$
Z	4	2	2
λ (Å)	0.71073	0.71073	0.9224
T (K)	100 (2)	400 (2)	423
Cell parameters			
a (Å)	10.1759(7)	4.9795(10)	4.9968(1)
b (Å)	4.9784(4)	4.9795(10)	4.9968(1)
c (Å)	10.2142(11)	9.727(3)	9.6911(3)
β (°)	115.687(1)	90(0)	90 (0)
V (Å^3)	466.31(7)	241.19(10)	241.97(11)
ρ (g/cm^3)	6.247	6.039	6.019
μ (cm^{-1})	142.5	137.74	265.84
$R(f)^a$	0.0220	0.0460	0.01
$R_w(f^2)^b$	0.0595	0.0713	0.019

[a]$R(F) = \sum||F_0| - |F_c||/\sum|F_0|$ for $F_0^2 > 2\sigma(F_0^2)$. [b]$R(F_0^2) = \{\sum[w(F_0^2 + F_c^2)]/\sum wF_0^4\}^{1/2}$.

Å for the same positions in the structure determined from the powder data (see Table 1). The V−O distances are 1.713 Å and 1.670 Å, as taken from the single-crystal and the powder diffraction analyses, respectively. Two thirds of the O−Ag−O bond angles of the tetrahedron at Wyckoff position 4d correspond to 100°, while the remaining third have a bond angle of 130°. At Wyckoff position 2b, two-thirds of the O−Ag−O bond angles correspond to 113°, while the remaining third have a bond angle of 102°. These distances are in good agreement with the value of 2.38 Å that is predicted from the Shannon radii of the ions, while the angles correspond closely to those found previously via powder diffraction.[13,39] The β-phase shows an inversion twin corresponding to 48% of the reflections, which is likely a consequence of the phase transition. Further details of the refinement can be found in the Supporting Information.

Stability Diagram of α-Ag_3VO_4. The theoretically calculated P_{O_2} vs T map illustrating the range of stability for α-Ag_3VO_4 is shown in Figure 1. This diagram was composed using the theoretically

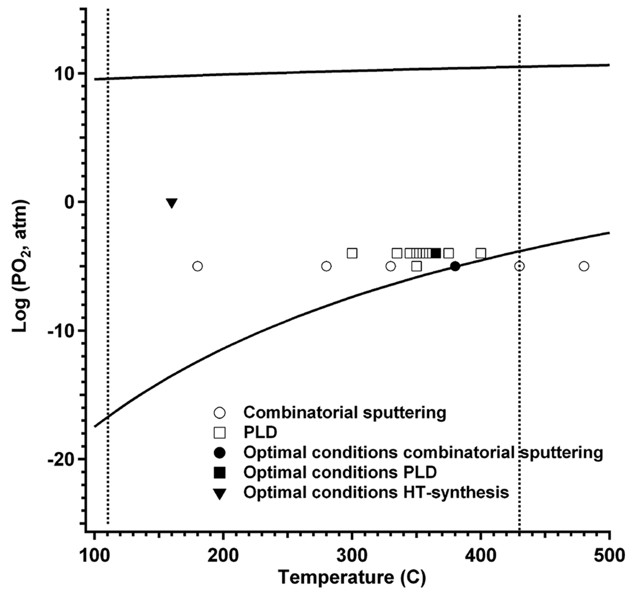

Figure 1. Thermodynamic stability diagram of α-Ag_3VO_4, as a function of experimental parameters. Dashed lines indicate phase-transition temperatures from α-Ag_3VO_4 to β-Ag_3VO_4 and from β-Ag_3VO_4 to γ-Ag_3VO_4. The conditions used for sputtering (circles), hydrothermal synthesis (triangle), and PLD (squares) are displayed on the graph. Filled markers indicate the presence of α-Ag_3VO_4, and open markers indicate the presence of secondary phases.

calculated minimum and maximum oxygen chemical potential data obtained from the thermodynamic stability plot presented by Trimarchi et al.[17] and the ideal gas law, as described by Osorio-Guillen.[40] Only thermodynamic effects, no kinetic effects, involved in α-Ag_3VO_4 formation were included in the construction of the diagram (Figure 1). The correspondence between the predicted and experimental growth conditions (deposition temperature, the cation ratio, and the partial oxygen pressure) of α-Ag_3VO_4 are described below.

Influence of Growth Temperature. Powder XRD analysis showed that the product of the low-temperature hydrothermal synthesis was polycrystalline α-Ag_3VO_4 (Figure 2). The hydrothermal synthesis was performed at 160 °C, which was within the temperature stability range of β-Ag_3VO_4 (110−414 °C) (Figure 1). As a consequence of the low-temperature and reversible phase transition from α-Ag_3VO_4 to β-Ag_3VO_4, it cannot be excluded that, initially, β-Ag_3VO_4 was formed during synthesis and that it transformed to α-Ag_3VO_4 upon cooling. No reflections of β-Ag_3VO_4 are found in the XRD spectrum after synthesis. Repeated transitions between α-Ag_3VO_4 and β-Ag_3VO_4 do not affect the intensity of XRD reflections

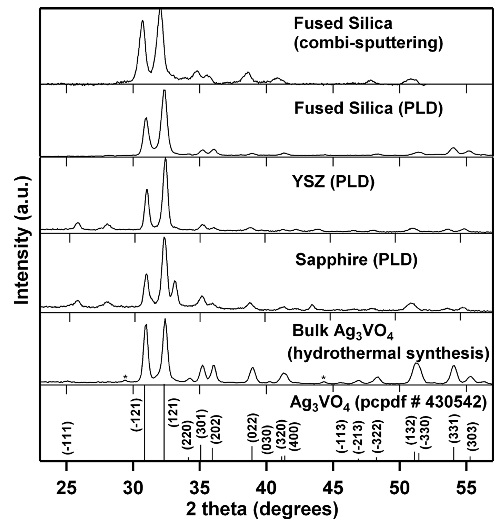

Figure 2. XRD patterns of α-Ag_3VO_4 thin film prepared by combinatorial sputtering (top) and pulsed laser deposition (PLD) (middle), compared to the polycrystalline powder (bottom) and the ICSD pattern. Stars indicate unknown impurities.

of α-Ag_3VO_4. These observations suggest that the transition is perfectly reversible and no significant quantities of β-Ag_3VO_4 are captured in the α-phase. From *in situ* XRD and optical analysis, it became apparent that the phase transition between β-Ag_3VO_4 and α-Ag_3VO_4 is very rapid and reversible. This could suggest that a phase transition might also occur during synthesis. The growth conditions of hydrothermally prepared Ag_3VO_4 fall within the boundaries of the theoretical predicted stability range.

The optimum deposition temperature for the combinatorial sputtered films was found to be 380 °C, which is higher than the hydrothermal growth temperature. A 50 °C deviation from this deposition temperature in both directions led to a significant increase of other phases. Significant reflections of Ag_2O or AgO were present in thin films deposited below 330 °C. Reflections of Ag, V_2O_5, and other vanadium-rich phases are observed in the films grown above 430 °C. In comparison to the thin films deposited by combinatorial sputtering, the ideal PLD deposition temperature range was found to be narrow. Keeping all other deposition parameters (P_{O_2}, target distance) constant, pure α-Ag_3VO_4 films could be grown only at temperatures of 350−365 °C (see Figure 3). At 300 °C, there was no sign of α-Ag_3VO_4—only Ag and V_2O_5 were present. However, at 335 °C, α-Ag_3VO_4 reflections appeared along with some V_2O_3 and an unidentified secondary phase. Above 370 °C, α-Ag_3VO_4 appeared to dissociate to Ag, V_2O_3, and V_2O_5. Differences in deposition mechanism and/or temperature calibration might account for the slight difference in optimal growth temperature between PLD and sputtering.

It is interesting to note that the optimal growth temperature range for pure α-Ag_3VO_4 thin films deposited via both thin film techniques was considerably restricted, compared to the theoretically calculated α-Ag_3VO_4 phase stability range (Figure 1). In contrast to the thin film deposition, hydrothermal synthesis of the polycrystalline powders and single crystals could be performed at much lower temperature. The kinetics of hydrothermal synthesis however are significantly different from vacuum techniques. The long synthesis time (24−48 h), low growth temperature (150−160 °C), and the liquid phase result in a very different distribution of chemical species.

Influence of Cation Ratio and Oxygen Partial Pressure. The stability of α-Ag_3VO_4 thin films made by combinatorial sputtering was strongly dependent on the cation composition ratio. Pure α-Ag_3VO_4 was expected to form at the stoichiometric composition ratio (V/(V + Ag) = 0.25), shown by the dashed line in Figure 4. The reflections of α-Ag_3VO_4 (at 30.8° and 32.2°) were observed in a broad range around V/(V + Ag) = 0.25, but pure α-Ag_3VO_4 was only present in a very

dx.doi.org/10.1021/cm301119c | Chem. Mater. 2012, 24, 3346−3354

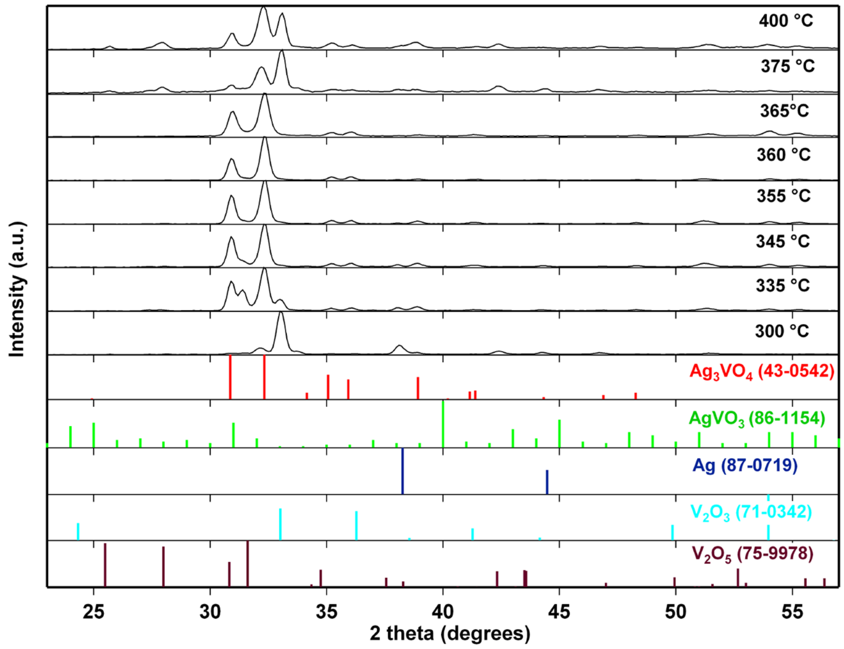

Figure 3. Crystallographic evolution of thin films deposited by PLD on fused silica as a function of deposition temperature under 150 mTorr of oxygen.

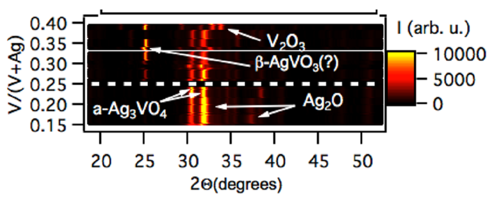

Figure 4. XRD intensity map of a compositionally graded sample grown by combinatorial sputtering (deposition at 380 °C and $P_{O_2} = 5 \times 10^{-6}$ atm). Dashed line indicates the ideal cation ratio for α-Ag_3VO_4.

small window (at V/(V + Ag) = 0.25). Secondary phases were observed on both sides of the ideal cation ratio (V/(V + Ag) = 0.25). At lower vanadium-content (V/(V + Ag) < 0.25), Ag_2O XRD reflections were present at 32.1° and 37.3°. At vanadium-rich compositions (V/(V + Ag) > 0.25), an unidentified vanadium-rich phase was observed in the XRD patterns at 25.6°, possibly β-$AgVO_3$. In addition, there was a weak reflection of V_2O_3 at 36.5°. These results are supported by the Ag_3VO_4 phase stability diagram that was calculated by Trimarchi et al.[17]

Interestingly, a comparison of XRD patterns illustrated that the excess Ag_2O that was found in the XRD patterns could be removed by wiping the thin film surface with a Kimwipe wet with isopropyl alcohol (not shown). This suggests that vanadium-poor samples (with respect

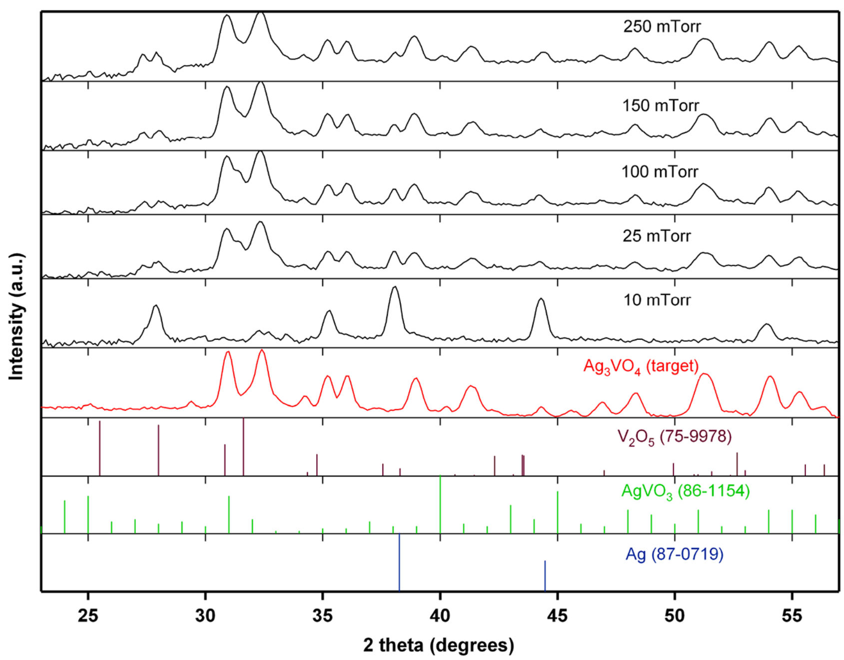

Figure 5. Evolution of XRD of thin films deposited by PLD on fused silica, as a function of oxygen partial pressure (P_{O_2}), deposited at 380 °C.

to α-Ag_3VO_4 composition) contained Ag_2O precipitates at the surface and vanadium-rich layers at the backside of the film. This observation was supported by SEM studies that confirmed Ag-rich regions at the surface. The composition of the thin films deposited by PLD between 340 and 360 °C were all near the stoichiometric ratio. At deposition temperatures below 340 °C, Ag_2O was predominantly present in the thin films, whereas the films deposited above 360 °C contained mostly V_2O_5.

The oxygen partial pressure (P_{O_2}) also played an important role in PLD deposition of α-Ag_3VO_4. As the oxygen partial pressure increased from 10 mTorr to 250 mTorr, Ag and V_2O_3 secondary phases initially disappeared, but reappeared at higher pressures (Figure 5). The oxygen partial pressure used for further deposition was 150 mTorr (Figure 1). As Figure 2 illustrates, the films deposited by PLD on the fused silica, YSZ, and sapphire were all polycrystalline in nature. There were small differences in the type of secondary phases present in the films. The films deposited on fused silica appeared to contain the least secondary phases, but also had the broadest reflections. When sapphire was used, a large V_2O_3 reflection at 33.01° and two reflections of V_2O_5 (at 25.4° and 27.9°) were found.

■ HIGH-TEMPERATURE XRD

The phase transition of Ag_3VO_4 in thin film samples was studied by *in situ* high-temperature powder XRD, as seen in Figure 6. One single sample was first heated continuously to

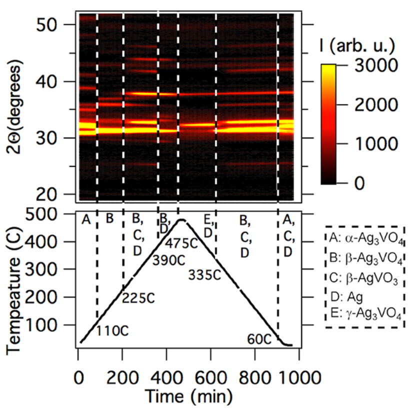

Figure 6. High-temperature XRD of thin film deposited by combinatorial sputtering (deposited at 380 °C and P_{O_2} = 5 × 10^{-6} atm) on a YSZ substrate.

450 °C and then cooled to room temperature. As described earlier, the phase transition from α-Ag_3VO_4 to β-Ag_3VO_4 occurs at 110 °C. Between 110 and 225 °C, only the β-Ag_3VO_4 phase is present, as observed from the strong intensities at 31.2°. However, upon heating beyond 225 °C, β-Ag_3VO_4 began to decompose to β-$AgVO_3$ and Ag metal. This irreversible process resulted in a permanent trace of Ag metal in the film (reflection at 37.8°). β-$AgVO_3$ transformed at 390 °C to a yet undefined phase, identified by the reflections at 30° and 33°. At 450 °C, β-Ag_3VO_4 transformed to the cubic γ-phase of Ag_3VO_4 (reflection at 32.28°) and Ag metal. Upon cooling, the reverse pathway took place and γ-Ag_3VO_4 consecutively transformed to β-Ag_3VO_4 and α-Ag_3VO_4 at 335 and 60 °C, respectively, with, as noted, a constant Ag metal presence. The transition temperatures were slightly lower during cooling, relative to the transition temperatures upon heating.

■ OPTICAL PROPERTIES

The onset of absorption of the orange α-Ag_3VO_4 pellet was measured at room temperature by diffuse reflectance spectrometry and was found to be 2.1 eV (Figure 7).[33] When α-Ag_3VO_4 transitions to β-Ag_3VO_4, the absorption edge of β-

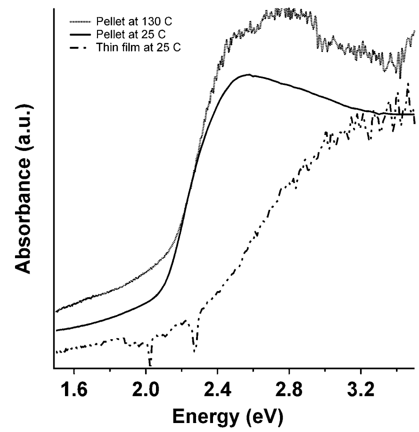

Figure 7. Absorption spectra of polycrystalline α-Ag_3VO_4 (measured at room temperature and at 130 °C) and thin film deposited by combinatorial sputtering.

Ag_3VO_4 was predicted to increase from 2.38 eV to 2.67 eV.[17] The measured onset of absorption corresponds best to the indirect band gap, because of the imperfect nature of the sample. Contributions of disorder, grain boundaries, and phonon-induced transitions lead to a decrease of the onset of absorption. To assess the onset of absorption of polycrystalline β-Ag_3VO_4, an *in situ* high-temperature diffuse reflectance analysis was performed. The change in absorption edge was the largest between room temperature and 130 °C. For clarity reasons, the spectra obtained at higher temperatures (above 130 °C) are omitted from the graph. As seen in Figure 7, the reflectance increased at the phase transition; however, the shift of the onset of absorption was minimal. Because the instability of β-Ag_3VO_4 precludes room-temperature measurements, the assessment of the β-Ag_3VO_4 absorption edge must be judged against the effect of the *in situ* high-temperature analysis. Taking into account the inversely related temperature effect on absorption edge, the experimentally observed increase was only slightly smaller (0.15 eV) than the theoretically predicted increase (0.3 eV).

The α-Ag_3VO_4 thin film was transparent and slightly yellow in color. The optical absorption map for the sample grown at 380 °C is shown in Figure 8. The absorption edge at 1.5 eV indicated the presence of Ag_2O at compositions below the α-Ag_3VO_4 composition (i.e., V/(V + Ag) < 0.25). Between V/(V + Ag) = 0.25 and 0.35, the absorption edge occurs at 2.2 eV, indicating that the vanadium-rich impurity present at this composition range (Figure 4) has an absorption onset higher

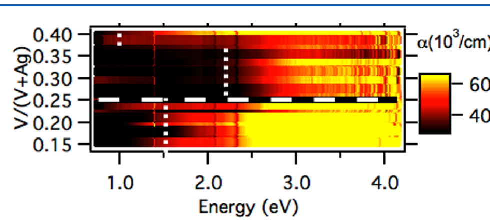

Figure 8. Optical absorption map of a Ag−V−O compositionally graded sample deposited by combinatorial sputtering (deposited at 380 °C and P_{O_2} = 5 × 10^{-6} atm). Vertical lines indicate absorption onsets of α-Ag_3VO_4 and secondary phases.

dx.doi.org/10.1021/cm301119c | Chem. Mater. 2012, 24, 3346−3354

than or equal to 2.2 eV. Given these observations, this secondary phase could be identified as β-$AgVO_3$, which was reported to have an optical band gap of 2.6 eV.[41] Figure 7 illustrates that the onset of absorption for α-Ag_3VO_4 thin films was comparable to the onset of absorption of the α-Ag_3VO_4 pellet. The contributions of disorder and phonon-induced transitions are smaller in thin films, compared to polycrystalline powder. However, grain boundaries and the film thickness still contribute to the decrease of the onset of absorption and indirect transitions cannot be excluded. Relatively high absorption values below the absorption onset in phase-pure thin films could be attributed to the scattering of light on the morphologically coarse thin-film samples. At higher vanadium contents (i.e., V/(V + Ag) > 0.35 in Figure 8), another absorption onset appeared, at ∼1 eV, which was most likely indicative of the presence of absorbing (black) V_2O_3. This observation is also consistent with the observation of an XRD reflection at V/(V + Ag) > 0.35 at 36.5°.

■ ELECTRICAL CONDUCTIVITY

The electrical conductivity and dielectric constants of the sintered Ag_3VO_4 pellet, obtained from the impedance spectroscopy measurements up to 365 °C, are shown as a function of temperature in Figures 9 and 10. Two main features are

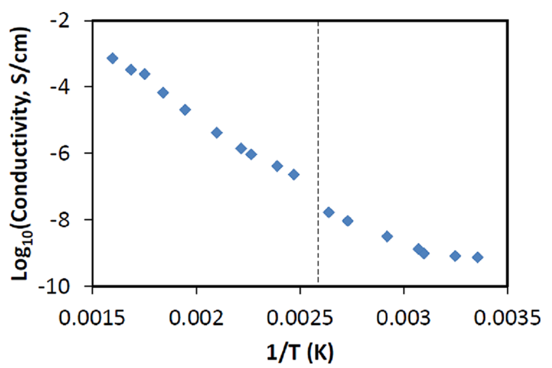

Figure 9. Electrical conductivity of polycrystalline Ag_3VO_4 pellet as a function of temperature. The dashed vertical line indicates the phase transition.

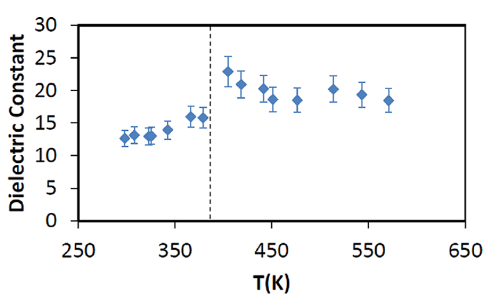

Figure 10. Dielectric constant of α-Ag_3VO_4 as a function of temperature. The dashed line indicates the phase-transition temperature.

apparent; the conductivity increases with increasing temperature, and there is a sharp increase in both conductivity and dielectric constant near the temperature reported for the phase transition from the low-temperature α-phase to the high-temperature beta β-phase (110 °C). This temperature is marked with a dashed line in Figures 9 and Figure 10. Thus, the electrical data appear to support the presence of this phase transformation and are consistent with the *in situ* XRD observations. It should be noted that the conductivity measured here with Ag electrodes is the total conductivity, which may be ionic (Ag^+ ions), electronic, or a combination of both. At room temperature the conductivity is as low as 10^{-9} S/cm, while above the phase transformation the conductivity ranges from 10^{-6} S/cm to 10^{-3} S/cm. These values are comparable to the total conductivity of other ternary silver compounds ($AgBO_2$,Ag_3BO_3, $Ag_2Ge_2O_5$, $Ag_6Ge_2O_7$, $Ag_6Si_2O_7$), as reported by Köhler et al.[4] The effective dielectric constant of the α-phase ranges from 13 to 16 with increasing temperature, and then reaches 19 for the higher-temperature β-phase. These dielectric constants are consistent with bulk values, rather than, e.g., a grain-boundary-dominated response, and support the interpretation of the impedance arc as a bulk feature.

α-Ag_3VO_4 thin films grown by combinatorial sputtering at 380 °C with V/(V + Ag) = 0.20−0.30 showed finite sheet resistance. As shown in Figure 11, in the vanadium-poor

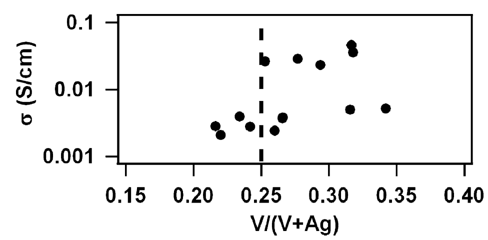

Figure 11. Electrical conductivity of compositionally graded film of α-Ag_3VO_4 deposited by combinatorial sputtering (deposited at 380 °C and P_{O_2} = 5 × 10^{-6} atm).

composition range (with respect to α-Ag_3VO_4 composition), the measured conductivity was 0.002−0.003 S/cm, whereas in the vanadium-rich composition, it was 0.2−0.3 S/cm. Such an increase at the α-Ag_3VO_4 composition could be attributed to an increase in concentration of Ag vacancies in this vanadium-rich region. Alternatively, the increase of electrical conductivity in the vanadium-rich composition range could be attributed to precipitation of β-$AgVO_3$ in this composition range (see Figure 4). However, such an interpretation is contingent on the fact that the measured sample contained no conductive secondary phases with very weak or no (i.e., amorphous) XRD reflections. One fact that places the origin of finite conductivity measurements in thin films in doubt is that the measured conductivity values were several orders of magnitude higher, compared to the results obtained using impedance spectroscopy on polycrystalline samples (Figure 9). In addition, the PLD-synthesized films did not exhibit any measurable conductivity. These results question the origin of the conductivity source and generate the need for phase-pure Ag_3VO_4 films.

■ CONCLUSION

Single crystals of α-Ag_3VO_4 were successfully grown via low-temperature hydrothermal synthesis. Single-crystal X-ray diffraction (XRD) was performed for the first time at elevated temperature and allowed us to refine the atomic positions of β-Ag_3VO_4. Because of the phase transition to α-Ag_3VO_4 below 110 °C, the optical and electrical properties of β-Ag_3VO_4 had to be measured using *in situ* elevated temperature diffuse reflectance spectroscopy and ac-impedance spectroscopy measurements. The polycrystalline pellet of Ag_3VO_4 exhibits an absorption onset at 2.1 eV. The onset of absorption of β-

Ag_3VO_4 increased slightly to 2.25 eV. This rather small increase can be attributed to the polycrystalline nature of the sample and the contributions from phonon-induced transitions, disorder, and grain boundaries. The observed change in conductivity between the α-phase and the β-phase was on the order of 3−6 orders of magnitude. However, even at the highest temperature, the absolute conductivity of β-Ag_3VO_4 remains low.

Because stabilization of β-Ag_3VO_4 in powder was not possible, attempts were made to grow room-temperature-stable thin films of β-Ag_3VO_4 by combinatorial sputtering and pulsed laser deposition (PLD). Thin film deposition of α-Ag_3VO_4 was successful, but β-Ag_3VO_4 could not be stabilized at room temperature. The experimental conditions that were required to deposit pure α-Ag_3VO_4 thin films were found to be sensitive to changes in deposition parameters. Small changes in temperature, composition, or oxygen partial pressure, quickly induced secondary phases such as Ag, V_2O_3, and V_2O_5. There was also little flexibility in the stoichiometry of α-Ag_3VO_4, with small deviations of the V/(V + Ag) = 0.25 immediately resulting in additional microcrystalline products. The onset of absorption of the thin film was very similar to the results obtained on pellets. The slight increased onset of absorption can be explained by the reduced amount of contributions from disorder and grain boundaries, in comparison to the pellet. However, indirect transitions will still take place in the 150-nm-thick film and therefore decrease the onset of absorption. Although the onset of absorption can be considered relatively low, transparency was obtained. Electrical properties of the thin films were difficult to measure: only the combinatorially sputtered thin film exhibited measurable conductivity. Therefore, the presence of other Ag−V−O compositions could be contributing to the measured values. Given the presented results, a conclusive answer on the *p*-typeness of α-Ag_3VO_4 and β-Ag_3VO_4 cannot be provided.

■ ASSOCIATED CONTENT

Supporting Information

The crystallographic data for Ag_3VO_4 at 100 and 400 K have been deposited with FIZ Karlsruhe as CSD Nos. 424347 and 424348, respectively. These data may be obtained free of charge by contacting FIZ Karlsruhe at +497247808666 (fax) or crysdata@fiz-karlsruhe.de (E-mail). This material is available free of charge via the Internet at http://pubs.acs.org.

■ AUTHOR INFORMATION

Corresponding Author

*E-mail: krp@northwestern.edu.

Notes

The authors declare no competing financial interest.

■ ACKNOWLEDGMENTS

This work was supported by the U.S. Department of Energy, Office of Science, Office of Basic Energy Sciences under Contract No. DE-AC36-08GO28308 to NREL. The "Center for Inverse Design" is a DOE Energy Frontier Research Center. The authors thank A. Korinda for assistance with the high-temperature diffuse reflectance, Dr. P. Parilla for assistance with the high-temperature XRD and Dr. C. Malliakas for his assistance with the high-temperature single crystal XRD. The authors also thank Dr. A. Zunger and Dr. S. Lany for valuable discussions. This work made use of the J. B. Cohen X-ray Diffraction Facility supported by the MRSEC program of the National Science Foundation (No. DMR-1121262) at the Materials Research Center of Northwestern University.

■ REFERENCES

(1) Hirono, T.; Yamada, T. *J. Appl. Phys.* **1984**, *55*, 781.
(2) Jansen, M. *Angew. Chem., Int. Ed.* **1987**, *26* (11), 1098−1110.
(3) Linke, C.; Jansen, M. *Inorg. Chem.* **1994**, *33*, 2614−2616.
(4) Kohler, B.; Jansen, M.; Weppner, W. *J. Solid State Chem.* **1985**, *57*, 227−233.
(5) Kumar, S.; Gupta, H. C. *Comput. Theor. Chem.* **2011**, *977*, 78−85.
(6) Ouyang, S.; Kikugawa, N.; Chen, D.; Zou, Z.; Ye, J. *J. Phys. Chem. C* **2009**, *113*, 1560−1566.
(7) Gessner, W. *Silikattechnik* **1970**, *21*, 45−46.
(8) Thilo, E.; Wodtcke, F. *Z. Anorg. Allg. Chem.* **1958**, *295*, 246−261.
(9) Klein, W.; Jansen, M. *Z. Anorg. Allg. Chem.* **2008**, *634*, 1077−1081.
(10) Masse, R.; Tordjman, I.; Durif, A. *Z. Kristallogr., Kristallgeom., Kristallphys., Kristallchem.* **1976**, *144*, 76−81.
(11) Newsam, J. M.; Cheetham, A. K.; Tofield, B. C. *Solid State Ionics* **1980**, *1*, 377−393.
(12) Friebel, C.; Jansen, M. *Z. Naturforsch., B: Anorg. Chem., Org. Chem.* **1984**, *39B*, 739−743.
(13) Dinnebier, R. E.; Kowalevsky, A.; Reichert, H.; Jansen, M. *Z. Kristallogr.* **2007**, *222*, 420−426.
(14) Hu, X.; Hu, C. *J. Solid State Chem.* **2007**, *180*, 725.
(15) Hirono, T.; Koizumi, H.; Yamada, T.; Nishi, T. *Thin Solid Films* **1987**, *149*, L85−L88.
(16) Albrecht, T. A.; Stern, C. L.; Poeppelmeier, K. *Inorg. Chem.* **2007**, *46*, 1704−1708.
(17) Trimarchi, G.; Peng, H.; Im, J.; Freeman, A.; Cloet, V.; Raw, A.; Poeppelmeier, K.; Biswas, K.; Lany, S.; Zunger, A. *Phys. Rev. B* **2011**, *84*, 165116.
(18) Hirono, T.; Yamada, T. *J. Appl. Phys.* **1986**, *59*, 948.
(19) Bertolini, J. *J. Emerg. Med.* **1992**, *10*, 163−168.
(20) Segal, E. *J. Chem. Health Saf.* **2000**, *7*, 18−23.
(21) Peters, D.; Miethchen, R. *J. Fluorine Chem.* **1996**, *79*, 161−165.
(22) Harrison, W.; Nenoff, T.; Gier, T.; Stucky, G. *Inorg. Chem.* **1993**, *32*, 2437−2441.
(23) Perkins, J. D.; del Cueto, J. A.; Alleman, J. L.; Warmsingh, C.; Keyes, B. M.; Gedvilas, L. M.; Parilla, P. A.; To, B.; Readey, D. W.; Ginley, D. S. *Thin Solid Films* **2002**, *411*, 152.
(24) Perkins, J. D.; Paudel, T. R.; Zakutayev, A.; Ndione, P. F.; Parilla, P. A.; Young, D. L.; Ginley, D. S.; Zunger, A.; Perry, N. H.; Tang, Y.; Grayson, M.; Mason, T. O.; Bettinger, J. S.; Shi, Y.; Toney, M. F. *Phys. Rev. B* **2011**, *84*, 205207.
(25) *Jade 2010, XRD Processing, Identification and Quantification*; Materials Data, Inc., 2010.
(26) *APEX 2 v.4.1*; Bruker Analytical X-ray Instruments, Inc.; 2011.
(27) *SAINT v.7.34a*; Bruker Analytical X-ray Instruments, Inc.; 2011.
(28) *SMART Data Collection v.5.054*; Bruker Analytical X-ray Instruments, Inc.; 2003.
(29) *SAINT Plus v.6.45a*; Bruker Analytical X-ray Instruments, Inc.; 2003.
(30) Stoe, Cie; IPDS Software. 1998
(31) Sheldrick, G. *Acta Crystallogr., Sect. A: Found. Crystallogr.* **2008**, *A64*, 10.
(32) Gelato, G.; Parthe, E. *J. Appl. Crystallogr.* **1987**, *20*, 4.
(33) Kubelka, P.; Munk, F. *Z. Tech. Phys.* **1931**, *12*, 593−601.
(34) Hwang, J.-H.; Kirkpatrick, K.; Mason, T.; Garboczi, E. *Solid State Ionics* **1997**, *98*, 93−104.
(35) Boukamp, B. A. *University of Twente, The Netherlands/WisseQ*, 1986−2005.
(36) McLachlan, D.; Blaszkiewicz, M.; Newnham, R. *J. Am. Ceram. Soc.* **1990**, *73*, 2187−2203.
(37) Schroder, D. *Semiconductor Material and Device Characterization*; John Wiley and Sons: Hoboken, NJ, 2006.
(38) Andrews, D.; Gianola, A.; Lineberger, W. *J. Chem. Phys.* **2002**, *117*, 4074.

(39) Shannon, R. *Acta Crystallogr., Sect. A: Cryst. Phys., Diffr., Theor. Gen. Crystallogr.* **1976**, *A32*, 751−767.
(40) Osorio-Guillen, J.; Lany, S.; Barabash, S.; Zunger, A. *Phys. Rev. Lett.* **2006**, 107203.
(41) Konta, R.; Kato, H.; Kobayashi, H.; Kudo, A. *Phys. Chem. Chem. Phys.* **2003**, *5*, 3061−3065.

■ NOTE ADDED AFTER ASAP PUBLICATION

This article was published ASAP on August 10, 2012, with minor text errors. The correct version was published ASAP on August 17, 2012.